ISSN 1027-4510, Journal of Surface Investigation: X-ray, Synchrotron and Neutron Techniques, 2025, Vol. 19, No. 1, pp. 224–237. © Pleiades Publishing, Ltd., 2025.

Fabrication and Optical Characterization of Ultrathin Graphene Oxide Films Using a Combination Technique of Layer-by-Layer Coating Methods

M. M. Saadeldin[a], *, Ahmed Samir[a], **, and A. Guirguis[b]

[a] *Physics Department, Faculty of Science, Cairo University, Giza, 12613 Egypt*

[b] *Basic Science Department, Faculty of Engineering, the British University in Egypt, Cairo, 11837 Egypt*

**e-mail: mohamedantfox@yahoo.com*

***e-mail: mmmounir@sci.cu.edu.eg*

Received August 31, 2024; revised October 11, 2024; accepted October 11, 2024

Abstract—The synthesis of graphene and graphene oxide (GO) is critical for unlocking their vast potential across a range of practical applications. Among the various methods employed, graphite exfoliation emerges as one of the most straightforward techniques for producing these materials. However, achieving optimal synthesis conditions, preserving the pristine structure, minimizing layers and lateral size, and reducing oxygen content present significant challenges. In this study, we focus on fabricating uniform GO thin films utilizing the intrinsic self-alignment phenomenon between scattered nanosheets, achieved through the exfoliation technique without the need for catalysis or templates. This innovative approach harnesses the natural properties of GO materials, making them more suitable for industrial applications. The electrical and optical properties of the resulting GO thin films were thoroughly characterized using microscopy, spectroscopy, and ellipsometry techniques. By classifying GO bulk material based on its electronic properties, it can be categorized as a high-energy gap semiconducting material due to the presence of both sp^3 and sp^2 bonds, along with abundant oxygen functional groups in its matrix. This characteristic allows for the tuning of the energy gap by controlling the oxidation/reduction level. Our findings reveal that the GO thin film with eight layers (GO_8) exhibited a superior self-alignment rate compared to other films, displaying fewer defects between GO nanosheets. This GO_8 thin film displayed semiconducting behavior with a confined bandgap value of 2.26 eV, as determined through optical measurements. The observed self-alignment phenomenon among GO nanosheets holds promise for engineering these scattered nanosheets into more complex nanostructures, potentially enabling various applications across different fields. This study highlights the importance of understanding and harnessing inherent material properties for the development of advanced materials with tailored functionalities.

Keywords: graphene oxide, thin-film, self-alignment, optical constants

DOI: 10.1134/S1027451025700338

1. INTRODUCTION

The potential of two-dimensional graphene oxide (GO) applications is growing every day in the scientific research centers and on the industrial level [1]. This is because it provides applicable solutions for tackling natural graphene challenges, for instance, a high-hydrophobicity [2], and the limited-scale production [3]. Several synthesis routes have emerged to provide a sufficient amount of GO materials for the industry [4, 5]. The exfoliation process is the most common methods to synthesize the GO materials with a large quantity, which usually occurs by intercalating the oxygen molecules through the three-dimension graphite matrix to increase the interlayer spacing between graphite layers [6]. The current manufacture processing of GO material successes to prepare few or double layers of graphene with a high yield [7]. Unfortunately, these irregular shapes GO sheets, with a wide range of lateral size are generated without any measure to control the synthesis process. Graphene derivatives e.g. graphene oxide (GO) and chemically-converted graphene (CGG) have also a wide range of thickness which can be tuned by altering the preparation technique from sub-nanometer of 0.3 nm [8] up to a few tens of nanometer, nearly 18 nm [9] and may be prepared from either single or few layers of graphene respectively. Moreover, these derivatives have different surface chemistry, for instance, GO material consists of 60% of carbon atoms are covalently bonded, whereby together via sp^3 hybridized in its lattice with oxygen-decorating functional groups, which are distributed on the basal plane (epoxy and hydroxyl groups) while others on the edges (carboxylic groups)

[10]. Such these properties play a significant role in their electronic properties [11]. Despite these beneficial characteristics of GO substance, the usage of GO derivatives remains restricted in optoelectronics applications compared to another graphene, which is prepared by Epitaxial Chemical Vapor Deposition (CVD) technique [12]. The reason behind that, the challenge to recombine these generated scattered GO nanosheets from theexfoliation reaction in a well distinct arrangement i.e. thin-film with no template or catalytic layer because any external materials would change the natural physico-chemical properties of GO thin-film [13]. Several attempts have been proposed to prepare a uniform GO thin-film by simple techniques such as dipping [14], spraying [15], and vacuum-filtrating [16]. However, the layer-by-layer self-assembled (LBL) technique [17] has demonstrated various advantages with the carbon materials, for example, carbon nanotubes (CNT) such as the thermodynamic stability, self-repairing, and controlled management of the structure [18]. In addition, the spin coating technique (SC) uses to control the thickness of deposited film through tuning few parameters, for instance, the aqueous solution concentration, adhesive nature of substrate treatment, and the spinning speed [19]. The electrical and optical properties of GO thin-film have revealed by several techniques such as Microscopy [20, 21], Spectroscopy [21, 22], and Ellipsometry [23–25]. The classification of GO bulk material according to its electronic properties, it can be categorized as the high energy gap semiconducting materials, due to the presence of the combination of sp^3, sp^2 bonds and rich-oxygenous functional groups in its matrix. Therefore, the energy gap of GO material could be tuned via controlling the oxidization/reduction level of the graphene oxide [26].

In this work, a simple preparation method is reported to synthesize a large-scale GO thin-film with minor defects i.e. mismatching, or imperfection between GO grain boundaries. At the nanoscale level, the GO nanosheets exhibited a self-alignment behavior due to their electrostatic forces toward each other, which help them to combine them in a successful layer. This self-alignment attitude may be attributed to the high-oxidization level, and the shrinking of the lateral size of GO sheets. To the best of our knowledge, it is the first time to report the natural self-alignment behavior between the GO nanosheets with no catalysis [27]. Furthermore, the preparation conditions, characterization, homogeneity via using atomic force microscope (AFM), the stability of deposited GO thin-film against different types of solvents and the optical characteristics of the prepared ultrathin GO films are discussed.

2. EXPERIMENTAL DETAILS

2.1. Chemicals

Graphite powder with particle size 20 μm, Sulfuric acid H_2SO_4 (98%), Ortho-phosphoric acid H_3PO_4 (85%), Potassium magnesium oxide $KMnO_4$ (98%), pure Ethanol alcohol (99%), Distilled water H_2O, Hydrochloric acid HCl (33%) and Hydrogen peroxide H_2O_2 (30%).

2.2. Synthesis of Graphene Oxide Dispersion Solution

A dispersion solution of GO material prepared by the oxidation process of natural graphite powder according to a modified Hummer's method [28]. Briefly, a (1 g) graphite powder mixed with a highly concentrated mixture solution of (360 mL) H_2SO_4 and (40 mL) H_3PO_4 acids and stirred for 60 min at room temperature then a (6 g) potassium permanganate added slowly with a limitation to remain the surrounding temperature ≤20°C. These oxidation agents were selected to providing as much as possible of oxygen sources during the exfoliated process and increasing the oxidization level of GO sheets. The reaction system was remaining under vigorous stirring for 4-day until its colour changed to be shadowy brown. The mixture poured to a freezing solution of a (400 mL) distilled water with (3 mL) H_2O_2 (30%). The colour of the solution turned from darkish brown to bright yellow (Canary). The solution was centrifuged and solid collected at 10000 RPM for 10 min. The solid was washed several times by (5L, 10% of HCl) solution to remove the unwanted minerals which produced from the reaction, that followed by washing with the plenty of deionized (DI) water. The resultant solid was filtrated by a PTFE (0.45 μm) pore-size and dried in oven 60°C to avoid any thermal reduction. A 0.03 wt % GO solution was prepared in a mixture of DI water and Ethanol with a 1 : 1 ratio to increase the dispersion. The GO solution was sonicated for 30 min by the homogenizer (VCX 750 model, pro-scientific company). The sonication duration was adjusted to breakdown the GO sheets to smaller sizes with the aim of minimizing the lateral size.

2.3. Graphene Oxide Thin-film Growth

A glass substrate was cleaned by a series of solvents (Acetone, Ethanol and DI water) in the bath sonication for 5 min for each separately, and then dried well in an oven at 100°C. The substrate was covered with a fixed amount (2 mL) of prepared GO of solution each run, then left for 2 min before running the spin coating unit. The spin coating adjusted on 500, 800, and 1600 RPM for 30-s each for spreading GO nanosheets. The layer was dried directly by hot air that is mounted over the sample at 70°C for 10-min. The whole process repeated several times to accumulate more layers over each other with the same mechanism as illustrated

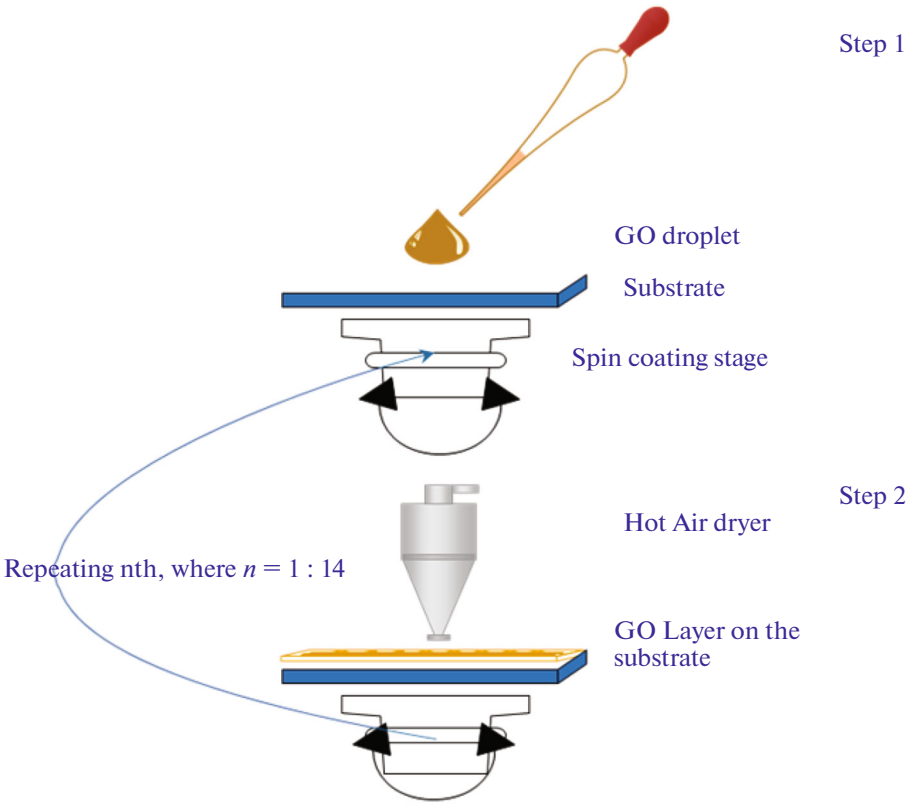

Fig. 1. A schematic mechanism of thin-film GO growth process.

in Fig. 1. For the reader simplification through this whole manuscript, we referred prepared GO films based on the number of layers, for instance, GO_6 means six layers of GO layers added. Three accumulation samples selected e.g., 6, 8, and 14 layers for conducting the optical study.

2.4. Characterizations

The GO crystal structure in powder and film form were examined by X-ray powder diffraction (XRD) using (X' Pert 1, Philips) diffractometer with a monochromatic source ($CuK_{\alpha 1}$) by 0.154 nm wavelength. All XRD patterns were recorded with a scanning rate of 40-ms and a 2-hr counting time. The functional groups of prepared graphite, as-produced GO powder were revealed via the Fourier-transform Infrared spectroscopy (FTIR) in the transmission mode by (FT/IR-4100, JASCO) between 400 and 4000 cm^{-1} wavenumbers. All optical measurements were recorded via UV-VIS Spectrophotometer (V-650, JASCO) from 190 to 4000 nm wavelengths. A dispersive Raman microscope (SENTERRA II, Bruker) with a laser source of wavelength 514 nm, 10% of laser power and 10-sec exposing time through 50 × 1000 μm aperture setting were used to confirm the graphitic structure of the GO layer. Scan electron morphologies were acquired via the Scanning Electron Microscope (SEM) (NeoScope Benchtop, JEOL) model at an accelerating voltage of 20 kV and a working distance of ~9 mm. Atomic Force Microscope (AFM) scanning was performed using a (Wet–SPM9600, SHIMADZU) in a static mode for the AFM mapping and imaging. The topography mapping was carried out on three different spots for each sample, with a scan rate of 0.5-Hz, and scan size of 1 μm at 512 samples/lines.

3. RESULTS AND DISCUSSIONS

3.1. Crystal Structure Investigation of GO Material

X-ray diffraction (XRD) patterns of GO nano-powder and thin-film were analyzed over a range of angles (2θ°) from 5° to 80°, as depicted in Fig. 2a. The pattern revealed that the as-prepared GO flakes exhibit crystallinity with a single sharp peak. The XRD spectra indicated that GO possesses a nano-crystalline hexagonal structure with lattice constants a = 2.4700 Å, b = 2.4700 Å, c = 6.7900 Å, according to card JCDPS (75-1621). Two major peaks corresponding to the (002) and (100) planes were observed for GO nano-flakes at 2θ values of 9.8° and 42.48°, respectively [29]. These planes correspond to an interlayer distance (d) of 8.39 Å, attributed to the stacked oxygen atoms between graphene sheets during the exfoliation process.

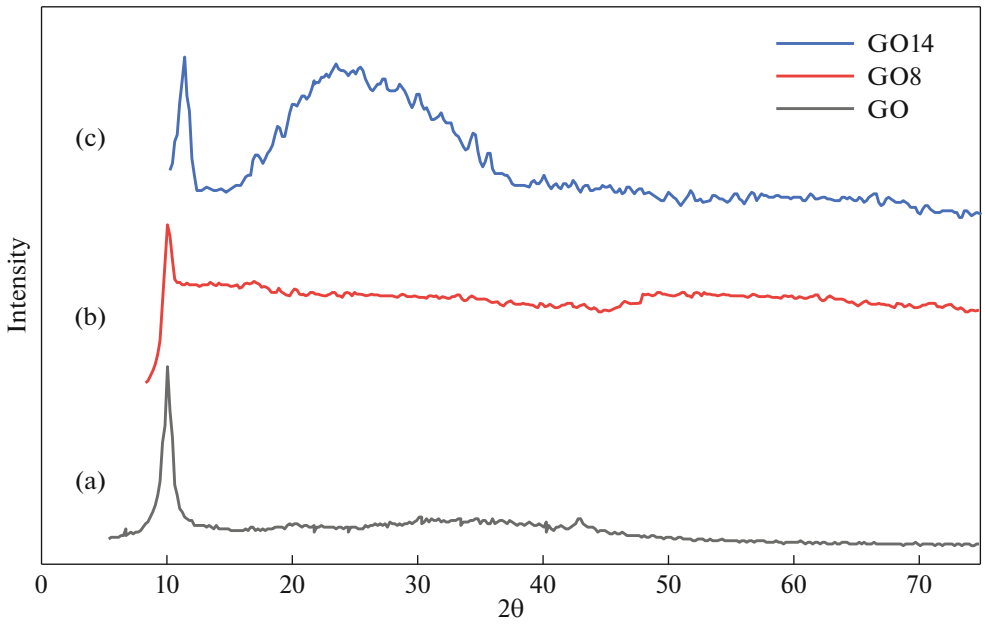

Fig. 2. X-ray diffraction patterns (a) as-produced GO powder, (b) thin-film (GO_8), and (c) thin-film (GO_{14}).

The crystal structure of the GO material was further confirmed using the diffraction pattern of the thin-films (GO_8) and (GO_{14}), as shown in Figs. 2b, 2c. Similarly, the maximum X-ray intensity was observed at $2\theta = 10.7° : 11.8°$, confirming that the film maintains the same structure as the GO powder without any impurities or contaminants.

The average crystallite size (D) was calculated from the XRD patterns of the GO powder, GO_8, and GO_{14} thin-film using the Debye-Scherer equation [30]. The calculated crystallite sizes at the (002) plane were approximately 8.2, 3.19, and 7.99 nm for GO powder, GO_8, and GO_{14} thin-film, respectively, indicating that the GO crystallite size falls within the nanometer range.

Additionally, two solid-state parameters, the dislocation density (δ) and strain (ε), were determined for the XRD spectra of GO powder and thin-film (GO_{14}) using specific equations. The dislocation density δ provides information about the disorder or defects in GO's lattice, while the strain ε indicates stress levels in the lattice material [31]. A comparison between GO nano-powder and thin-film (GO_8) based on crystallite size (D), dislocation density (δ), and strain (ε) parameters are presented in Table 1.

$$\delta = \frac{n}{D^2}, \tag{1}$$

$$\varepsilon = \frac{\beta}{4\tan\theta}. \tag{2}$$

The dislocation density of the thin-film (GO_8) was 6 times that of the as-produced GO powder, likely due to the spreading of GO nanosheets over the substrate. Additionally, the strain of the thin-film (GO_8) was 2 times that of the GO powder, suggesting the distribution of GO sheets with some morphological imperfections between boundaries.

3.2. Spectroscopy Analysis via FTIR and Raman

FT-IR spectrum for natural graphite powder and as-produced GO powder was measured over a range of wave numbers from 400 to 4000 cm^{-1} as shown in Fig. 3. The transmittance pattern shows the following distinguish functional groups of GO nano-powder as following: C–O–C (1.037 cm^{-1}), C–O (1.207 cm^{-1}),

Table 1. A comparison between the as-produced GO powder, GO_8, and GO_{14} according the average crystallite size D, d-Spacing, strain ε and dislocation density δ parameters

Sample	2θ°	β, deg	D, nm	d-Spacing, Å	ε	δ, nm^{-2}
GO	10.53°	1.039	8.02	8.39	0.049	0.0155
GO_8	10.71	2.61	3.19	8.25	0.12	0.098
GO_{14}	11.8	1.043	7.99	7.49	0.044	0.0156

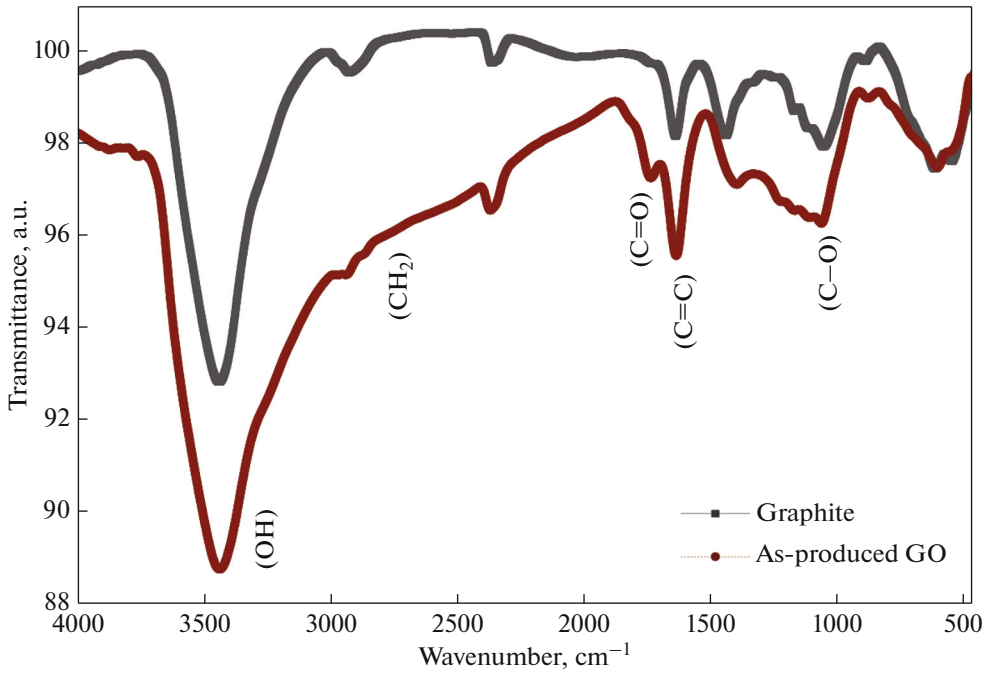

Fig. 3. FTIR-spectra of natural graphite powder and as-produced GO powder.

C=C (1.627 cm^{-1}) and C=O (1.726 cm^{-1}) bonds. Two primary peaks were observed at 3437 and 2920 cm^{-1} corresponding to O–H and CH_2 stretching vibration modes respectively, which match with the literature [32].

Raman microscope was employed to examine the graphitic structure of the thin-film (GO_{14}). The spectrum showed a G-band at (1.600 cm^{-1}), D-band at (1.345 cm^{-1}) and 2D-band at (2.700 cm^{-1}) as illustrated in the Fig. 4. It is well-known that The G-band is corresponded to scattering from graphitic carbon, whereas the D-band is related to the lattice's disorder in graphene planes [33]. The characteristic ratio between Raman's bands (I_{2D}/I_G) intensities of mono, double, triple, or more layer of graphene is reported to be > 1.6, ~0.8, ~0.30, or ~0.07 respectively [34]. In this work, the I_{2D}/I_G intensity ratio for as-produced thin-film (GO_{14}) was calculated ~ 0.12. This may mean that the structure of the thin-film is consisted of either more than ten layers of graphene oxide due to the GO accumulation or may be less than that due to the presence of functional groups between GO layers happened during the growth process. Furthermore, the in-plane crystalline size was calculated via empirical equation [35]. The obtained L_a value was around 21 (nm), which is agreed with previous literature for multilayer graphene oxide [36].

$$L_a = 2.4 \times 10^{-10} (\lambda_{laser}^4) \left(\frac{I_D}{I_G}\right)^{-1}, \quad (3)$$

where λ_{laser} is the wavelength of the laser used during the Raman test, I_D and I_G are D-band and G-band intensities respectively.

3.3. Morphological Structure of Ultrathin Films

3.3.1. SEM images. Figure 5 provided information describes SEM images of graphene oxide (GO) thin-films of GO_6, GO_8, and GO_{14}. Here's an explanation of the details: The SEM images offer a visual representation of the morphology and distribution of GO nanosheets on the substrate. GO_6 thin-film is described as maintaining an adequate distribution of GO nanosheets, suggesting a relatively uniform coverage over the substrate surface. In contrast, GO_8 thin-film exhibits a higher regularity, indicating a more pronounced self-alignment rate between the GO sheets on the substrate surface. This suggests that the nanosheets in GO_8 are aligned in a more ordered manner compared to GO_6. GO_{14} thin-film shows the lowest distribution, with the presence of imperfections such as wrinkles, cracks, pores, or lines observed between GO boundaries. This indicates that the GO nanosheets in GO_{14} are less uniformly distributed and may have fewer interactions between adjacent nanosheets.

3.3.2. AFM images. The Atomic Force Microscope (AFM) was utilized to analyze the surface morphology and roughness of ZTO/PVA films. Figure 6 presents 2D- and 3D-AFM representations of GO_6, GO_8, and GO_{14} films, with a surface scan size of 1.00 × 1.00 μm. Roughness parameters were determined and are

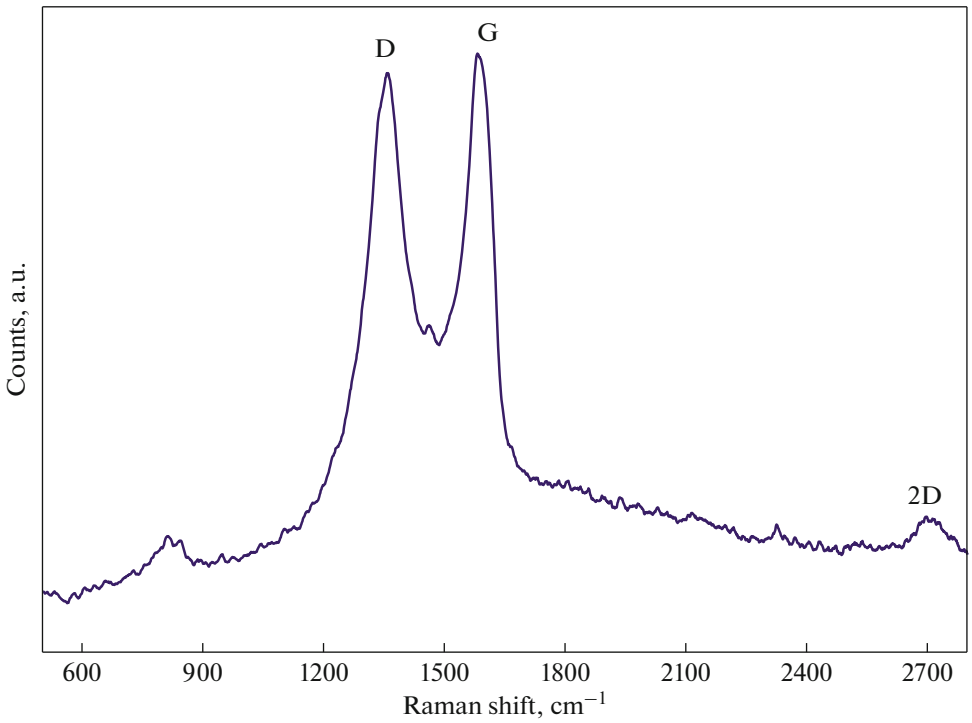

Fig. 4. Raman spectrum of as-produced thin-film (GO_{14}).

detailed in Table 2. The uniformity of GO films was assessed using AFM to obtain consistent statistics about GO bilayers, as shown in Fig. 6. The 3D morphology of GO_6, GO_8, and GO_{14} films is depicted in Fig. 6. Statistical representations derived from AFM scans of these films, including mean height, surface area, pattern width, and roughness factor, are presented in Fig. 7. The mean height of the GO films was measured as 6.89 nm for GO_6, 65.57 nm for GO_8, and 7.85 nm for GO_{14}. The discrepancy in film height evaluations may be attributed to the uncontrolled accumulation of multiple GO layers during the layering process. Regarding surface area, GO_8, exhibited the lowest value at 0.0010 μm^2, while GO_6 and GO_{14} had surface areas of 0.003 and 0.006 μm^2, respectively. Additionally, GO_8 showed the narrowest pattern width among the samples, while GO_{14} had the highest roughness value.

AFM measurements summarized in Table 2 in the supplementary materials provide further insights into the characteristics of these GO thin-films. In conclusion, the GO nanosheets were effectively assembled to form continuous layers, with GO_8, demonstrating the most satisfactory assembly quality, exhibiting minor imperfections between boundaries compared to GO_6 and GO_{14} films.

3.4. Homogeneity and Stability of Ultrathin GO Films using LBLS Approach

The UV-Vis spectroscopy was used to screen the development of GO multi-layer during the growth. Fig. 8 represents the transmittance coefficients of GO films from 1 to 14 bilayers on the glass substrate over three different wavelengths that including 488, 550, 633 nm. This graph illustrates a steady decay in the transmittance distributions corresponding three wavelengths, which is evidence of the successful accumu-

Table 2. Comparison between three graphene oxide films GO_{14}, GO_8 and GO_6 according to sheet width, average height, surface area, roughness, and distortion parameters GO_{14} films

Sample	Sheet width/nm	Mean height/nm	Surface area/μm^2	Roughness/a.u	Distortion/a.u
GO_{14}	66 ± 31	7.854 ± 1.689	0.006 ± 0.004	2.555 ± 1.181	0.44 ± 0.245
GO_8	22 ± 19	65.57 ± 6.039	0.001 ± 0.002	1.594 ± 0.896	0.538 ± 0.304
GO_6	39 ± 23	6.893 ± 1.228	0.003 ± 0.003	1.931 ± 0.87	0.397 ± 0.208

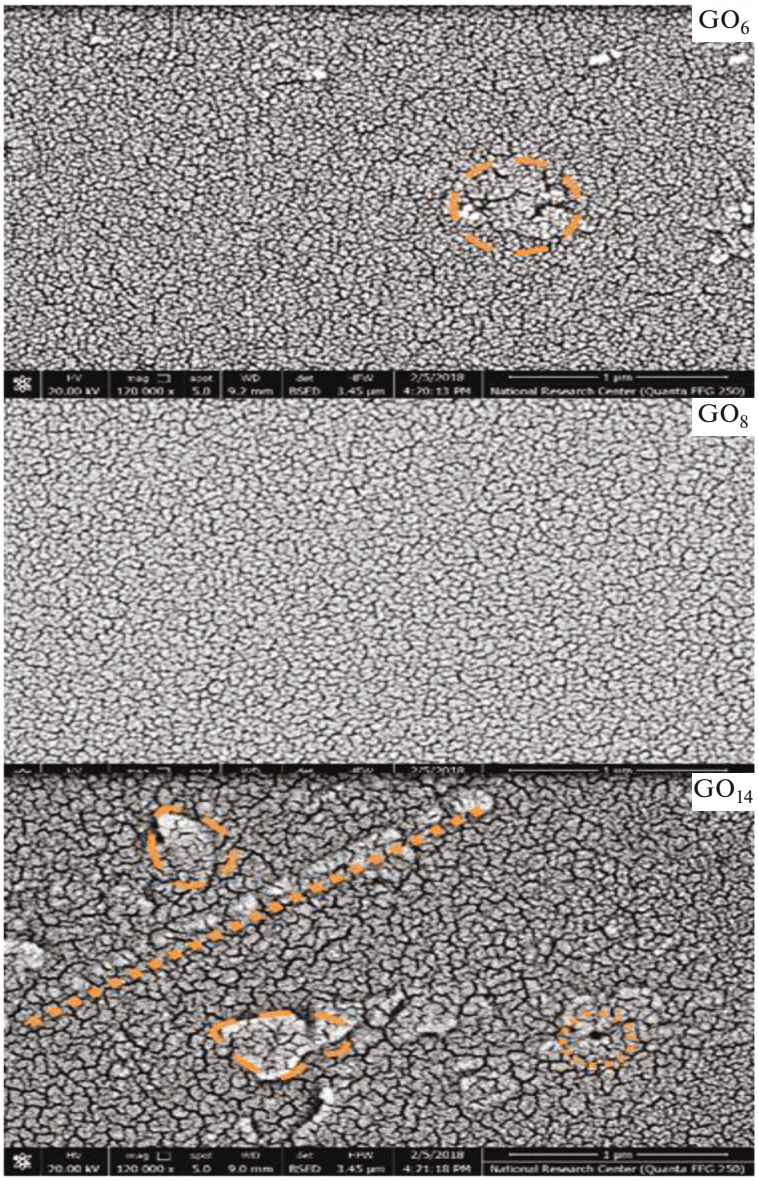

Fig. 5. SEM image of morphological structure of three GO films of (a) GO_6, (b) GO_8, (c) GO_{14}.

lating of thin GO layers over each other by adding bilayers. The stability of GO films was tested through immersing GO thin-films into several solvents including (DI) water, Ethanol, and a mixture of water and HCl with a ratio of (1 : 1) for a couple of days. All GO films have shown adequate resistance against toward these solvents.

3.5. Optical Properties Analysis

The influence of the self-aligned GO nanosheets over a transparent substrate (glass) on the optical response was consequently evaluated for three multi layers (6, 8 and 14-layer). Optical transmittance (T) and reflectance (R) of films are represented in Fig. 9a.

Table 3. Specific parameters regarding the optical constants of the three-thin film: GO_6, GO_8, and GO_{14}

Parameter/Sample	E_o	E_d	ε_∞	E_g, eV	ε_L	N/m^*, $kg^{-1}\,m^{-3}$
GO_6	3.69	9.89	1.84	2.12	3.39	1.51×10^{44}
GO_8	4.11	14.16	3.06	2.26	3.49	1.44×10^{44}
GO_{14}	3.87	15.53	4.73	3	3.53	1.34×10^{44}

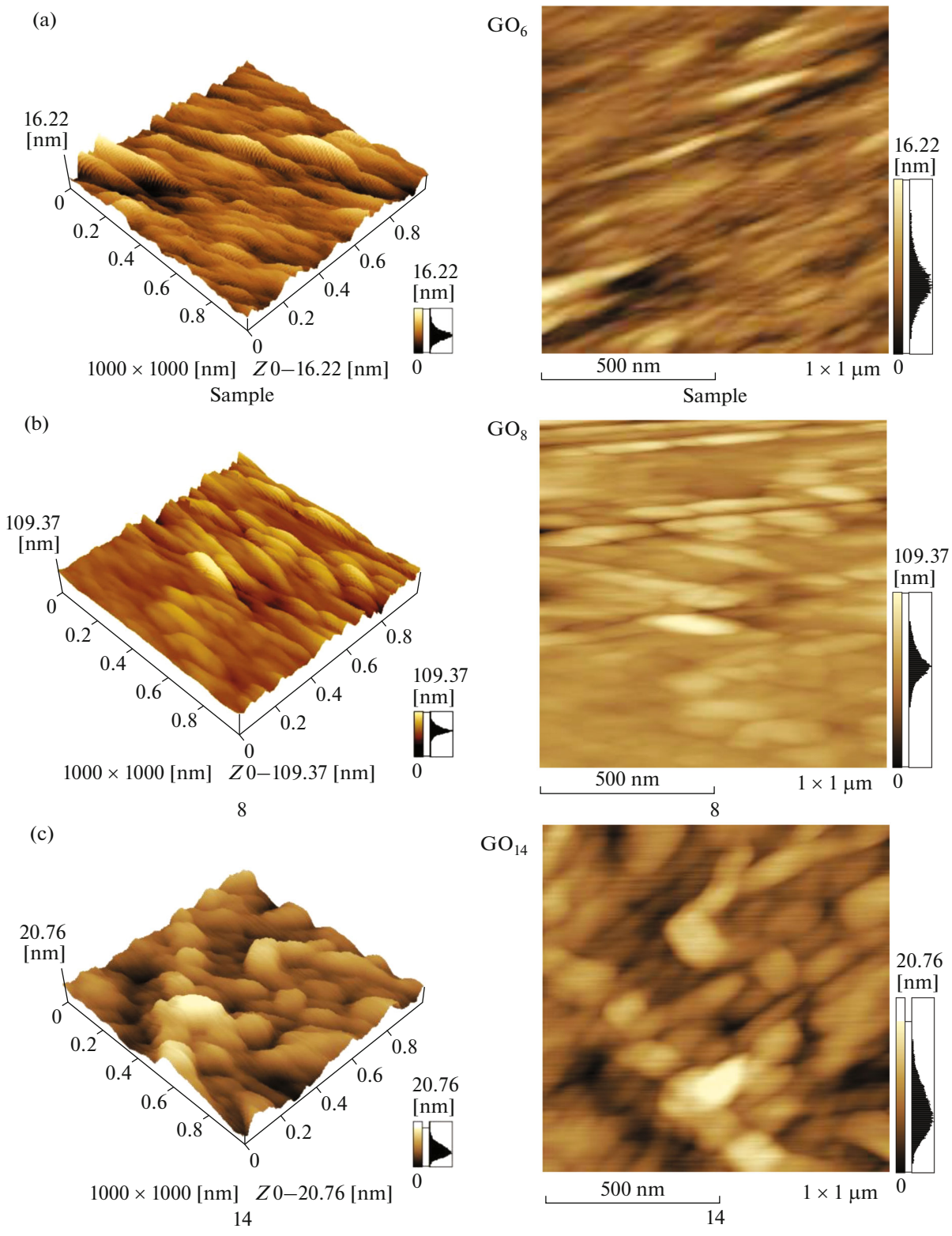

Fig. 6. AFM 2D and 3D topographic images to highlight homogeneity of ad-layer through the elevation distribution of graphene oxide sheets on the glass substrate (a) GO_6, (b) GO_8, (c) GO_{14}.

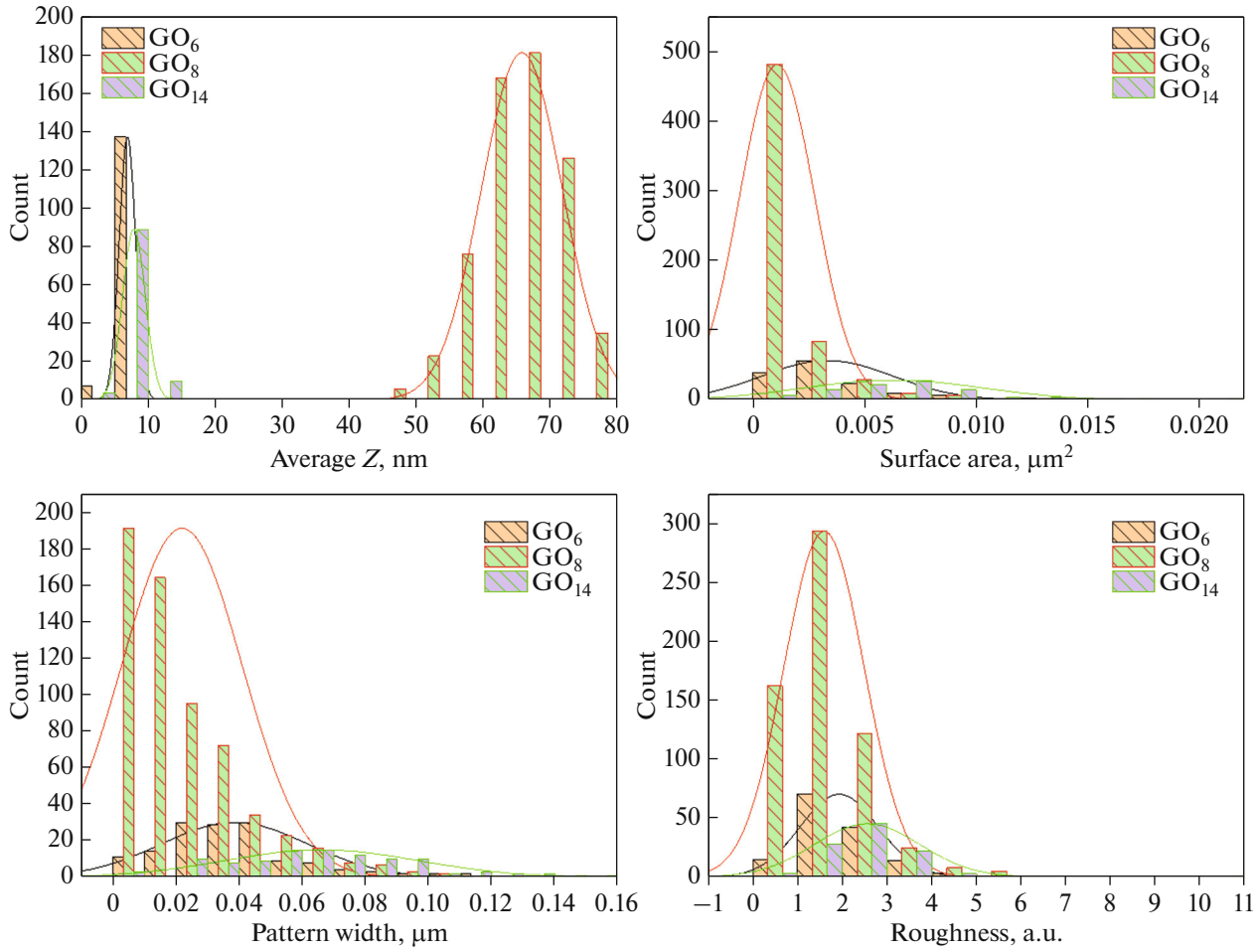

Fig. 7. Statistics histograms of average height, surface area, pattern width and Roughness for GO_6, GO_8, GO_{14} thin-films based on AFM records: — GO_6, — GO_8, — GO_{14}.

that used to compute absorption coefficients (α) for all of the samples via the empirical equation [38]:

$$\alpha = \frac{1}{d}\ln\left[\frac{(1-R)^2}{T} + \sqrt{\frac{(1-R)^4}{4T^2} + R^2}\right], \quad (4)$$

where (T) is transmittance, (R) is reflectance coefficients and (d) is the thickness.

The dependence of $(\alpha h\nu)^m$ on photon energy ($h\nu$) was plotted for different values of m according to the empirical equation [39]:

$$(h\nu\alpha)^m = A(h\nu - E_g), \quad (5)$$

where the parameter m considers the type of band gap transition considered specifically $m = 0.5$ and 2 for indirect/direct band transitions respectively. The best fit was obtained for $m = 2$ indicating the existence of direct transitions in all films under investigations as shown in Fig. 9b.

The Tauc plot was assessed to evaluate the semiconducting bandgap according to Eqs. (4) and (5). The inset figure in represents the dependence of E_g with GO different layers. These GO three-thin film acts as semiconducting layers which have both of sp^2 and sp^3 in its matrix. All GO thin-films showed a band gap in the range of 2.1–3 eV in a good agreement with reported values (2.1–2.8) eV in the literature [23, 24]. A minimum band gap was 2.1 eV assigned for GO_6 sample whereas the maximum bandgap was 3 eV for GO_{14} sample and the moderate band gap energy was 2.26 eV for the GO_8 sample. This is attributed to a couple of reasons. The first reason is the increasing oxygen functional groups that might act as electronic trips for lacking the free carrier movements and it can block the free π-covalent bonds between attached GO layers. Furthermore, the development of imperfections between grains which create localized states into the band gap [26, 40].

From the experimental values of T_{exp}, R_{exp}, and the film thickness d, the refractive index, n, and extinction coefficient, k, were assessed according to Murman's

exact equations [41] with a computerized routine targeting to minimizing $(\Delta T)^2$ and $(\Delta R)^2$ where:

$$(\Delta T)^2 = \left|T(n,k) - T_{\exp}\right|^2, \quad (6)$$

$$(\Delta R)^2 = \left|R(n,k) - R_{\exp}\right|^2, \quad (7)$$

where $T(n, k)$ and $R(n, k)$ are the calculated values of transmittance and reflectance, respectively, by routine. Two operations are accomplished in this search: (1) The bivariant search operation is to calculate $T(n, k)$ and $R(n, k)$ throughout of n_1 to n_2 and k_1 to k_2, finally, we get the optimum values of n and k simultaneously. (2) Step-length optimization operation is to expedite convergence to improve accuracy. For more details go to [42]. The values of n and k obtained at the minimum variances are noted as n_m and k_m. The values $[n_m - (n_2 - n_1)/10]$ and $[k_m - (k_2 - k_1)/10]$ are then compared to specific tolerance values ($t_n = 0.01$ and $t_k = 0.001$). The program will be ended if these values are smaller than the tolerance values, then $n = n_m$ and $k = k_m$. The calculations are repeated to obtain the equivalence if these values are higher than the tolerance values.

The refractive index, n was assessed from measured transmittance and reflectance coefficients according to Murman's exact [42]. Figure 9c shows the spectral distribution of the refractive index (n) as a function of (λ) for prepared GO thin-films. At the 600 nm, the highest n value was for the GO_{14} film around 2.6, while the GO_6 was the lowest at 2.2. Similarly, the GO_8 film exhibited a moderate 2.4 value for the refractive index in a good agreement with the reported values in the literature by other techniques such as microscopy [20] and spectroscopy [21]. The refractive index for both GO_6 and GO_8 has the same behavior to the light while GO_{14} showed an odd attitude especially near to the infrared region. These variations in the refractive index value for GO thin-films are considered as a piece of strong evidence that growth technique work effectively to accumulate GO layers over each other.

Wemple–DiDomenico relationship was computed for three-thin film as expressed [43].

$$\frac{1}{(n^2 - 1)} = \frac{E_O}{E_d} - \frac{(h\nu)^2}{E_O E_d}. \quad (8)$$

The values of oscillator parameters E_d and E_o can be determined from the intercepts and the slopes of the obtained straight lines of the relation between $1/(n^2 - 1)$ and $(h\nu)^2$ for GO films as shown in Fig. 10 and Table 3. These values E_d and E_o decreased with increasing film thickness. By extrapolating the linear part towards zero photon energy, the interception with y-axis can be utilized for the determination of the optical dielectric constant ($\varepsilon_\infty = n^2$), which summarized the Table 3.

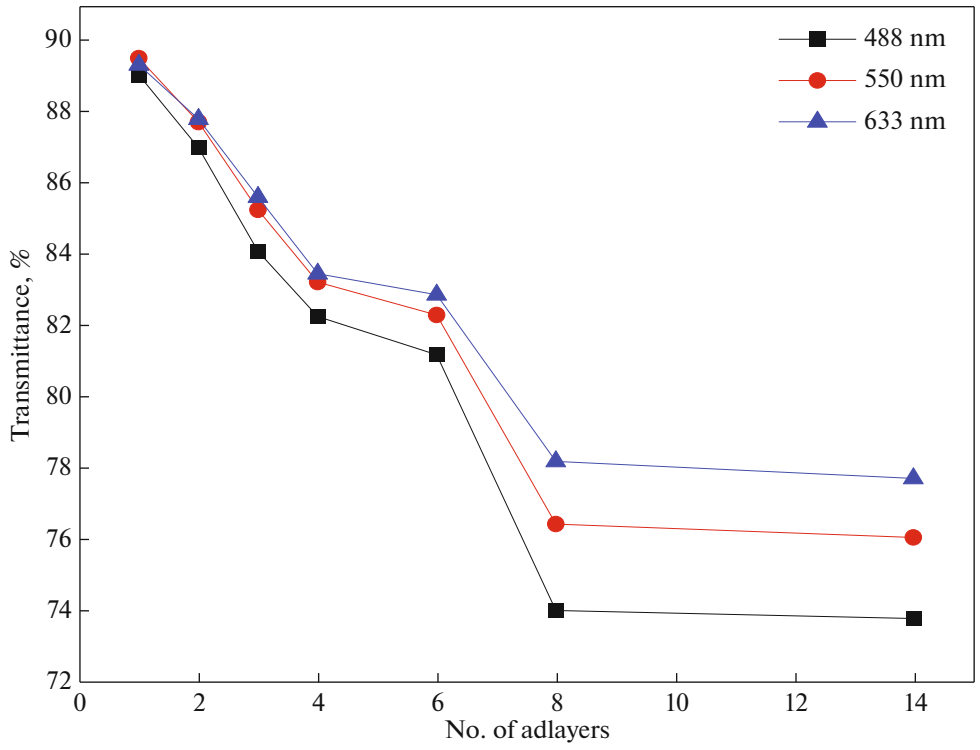

Fig. 8. The transmittance coefficients of films over three different wavelengths that including 488 nm (—), 550 nm (—), 633 nm (—) wavelengths.

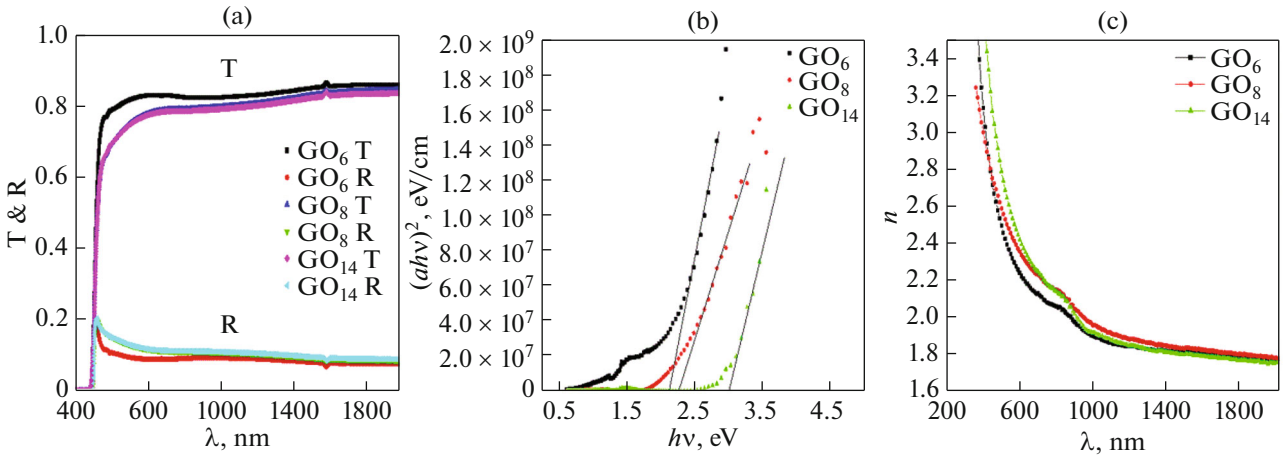

Fig. 9. Optical performance results for three GO thin-films: (a) spectral optical distribution of transmittance and reflectance, (b) the Tauc's relation for direct transitions. The inset figure represents the dependence of E_g, (c) spectral distribution of refractive indexes.

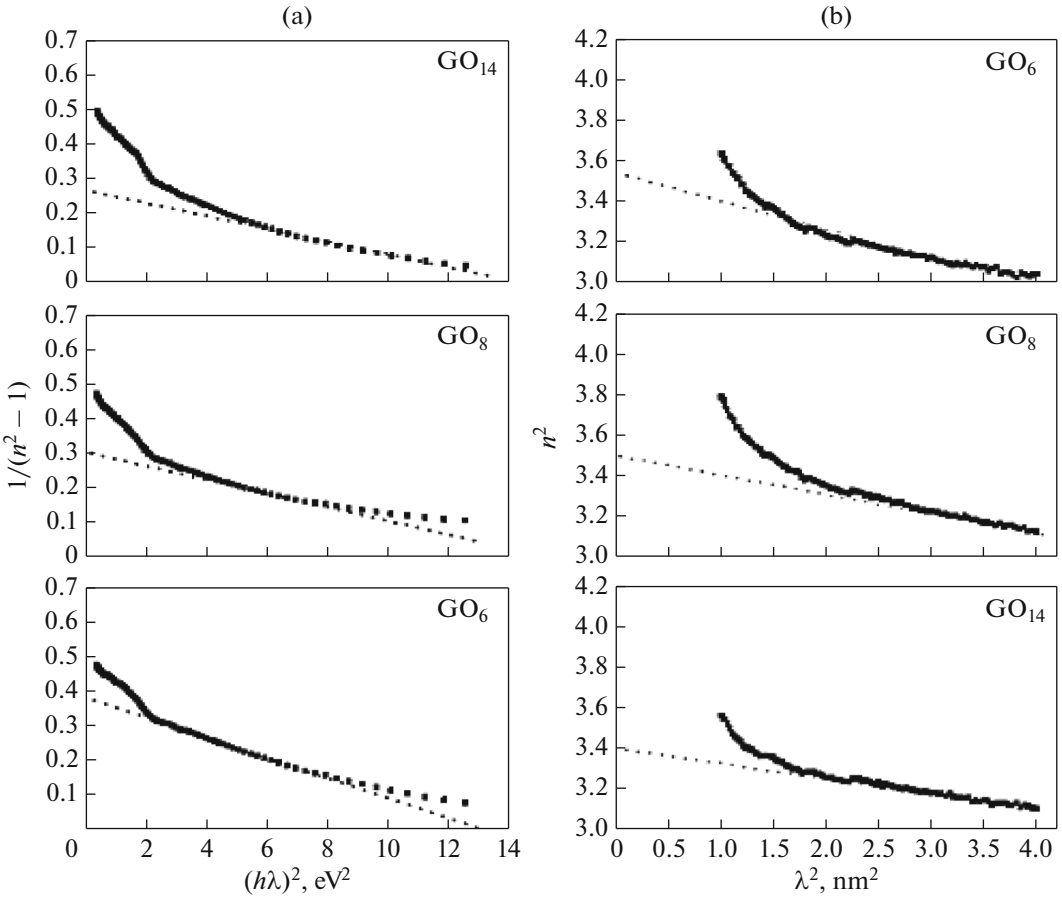

Fig. 10. (a) The relation between $(n^2-1)^{-1}$ and square of photon energy to GO different layers and (b). The relation between n^2 versus λ^2 for GO different layers.

The relationship between the lattice dielectric constant ε_L, and refractive index, n, also was calculated by [44]:

$$n^2 = \varepsilon_L - \left(\frac{e^2 N}{4\pi\varepsilon_o C^2 m^*}\right)\lambda^2, \quad (9)$$

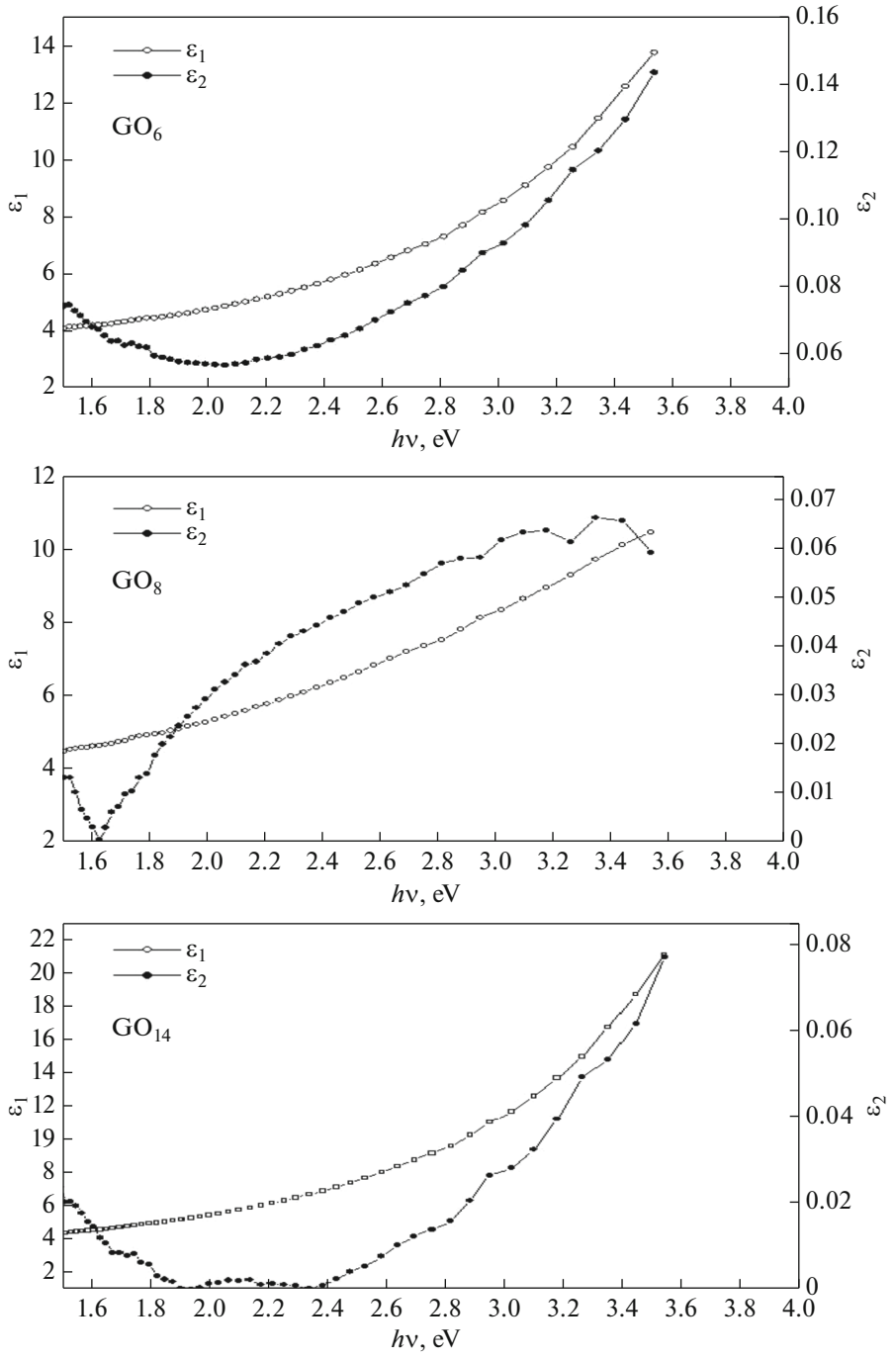

Fig. 11. Optical complex dielectric attitudes versus photon energy of three thin-films.

where ε_L is the lattice dielectric constant, N/m^* is the ratio of the carrier concentration to the effective mass, C is the speed of light, e is the electronic charge and ε_o is the permittivity of free space. The plot of n^2 versus λ^2 for GO films is demonstrated in Fig. 10b. The values of lattice dielectric constant are calculated from the intercepts and slopes of the straight lines in the Fig. 10b. and given in Table 3 with the values of N/m^* which was approximately constant for all prepared films.

The complex dielectric constant for three thin-films was assessed which is given by:

$$\tilde{\varepsilon} = \varepsilon_1 + i\varepsilon_2 \because \varepsilon_1 = n^2 - k^2 \;\&\; \varepsilon_2 = 2nk, \qquad (10)$$

where ε_1 and ε_2 are the real and imaginary parts of dielectric constant.

No significant variations in the ε_1 of dielectric constant values, whereas few distinctions in, ε_2 were revealed between three GO accumulations as pre-

sented in Fig. 6. Such changes in the ε_2 attitudes may be attitude to the phase difference between the electric field photons, suggesting inconsistency in the GO sheet alignment for both 6 and 14 accumulation during the growth A representative clarification, for example, the complex dielectric constant for thin-film (GO_6) demonstrated the relationship between ε_1 and ε_2 partswith the photon energy of the thin-film (GO_6). The ε_1 values are higher than that for the ε_2 values. The ε_1 is increased with the increase of energy portions whereas the ε_2 is decreased at lower energy range. The variation of ε_1 was attained due to its dependence on the n^2 value, whereas the k values was found to the variation of absorption coefficients [45, 46].

4. CONCLUSIONS

In this study, the FT-IR analysis of GO nano-powder revealed distinct functional groups, including C–O–C, C–O, C=C, and C=O bonds, as well as characteristic peaks corresponding to O–H and CH_2 stretching vibration modes. The calculated I2D/IG intensity ratio for the GO_{14} thin-film suggested a structure consisting of either more than ten layers of graphene oxide or fewer layers with functional groups between GO layers. Additionally, the in-plane crystalline size was determined empirically, and AFM measurements confirmed successful assembly of GO nanosheets into thin films, with the GO8 film demonstrating the most satisfactory assembly. The transmittance decay at three wavelengths indicated successful accumulation of thin GO layers over each other, providing evidence of layer-by-layer stacking. Furthermore, the stability of GO films was demonstrated through resistance testing against various solvents. The refractive index analysis showed variations among GO thin-films, with the highest value observed for GO_{14} and the lowest for GO_6, while GO_8 exhibited a moderate value consistent with literature reports. These variations are indicative of the effectiveness of the growth technique in accumulating GO layers. The observed variations in the optical properties and dielectric constants of GO films provide valuable insights into their behavior, shedding light on factors such as film thickness and alignment. These findings contribute to a better understanding of GO thin-films and can inform the design and optimization of graphene-based devices for diverse applications. Additionally, the demonstration of the natural self-alignment phenomenon in highly-oxidized two-dimensional carbon nanosheets highlights the potential for engineering complex nanostructures based on graphene materials.

ACKNOWLEDGMENTS

Authors appreciated Laser technology unit, Centre of Excellence for advanced sciences, National research center and Nanomaterial & Nanotechnology Dept., Advanced Materials Div., Central Metallurgical R & D Institute (CMRDI), P.O box 87, Cairo, Egypt for sharing their facilities in this research.

FUNDING

This work was supported by ongoing institutional funding. No additional grants to carry out or direct this particular research were obtained.

CONFLICT OF INTEREST

The authors of this work declare that they have no conflicts of interest.

REFERENCES

1. F. Zhang, W. Li, Y. Ma, and X. Dai, Solid State Commun. **271**, 56 (2018).
2. J. S. Bunch and M. L. Dunn, Solid State Commun. **152** (15), 1359 (2012).
3. L. Zhao, Kwang Taeg Rim, Kh. Chzhou, et al., Solid State Commun. **151** (7), 509 (2011).
4. W. S. Hummers Jr and R. E. Offeman, J. Am. Chem. Soc. **80** (6), 1339 (1958).
5. L. Staudenmaier, Ber. Dtsch. Chem. Ges. **31** (2), 1481 (1898).
6. S. Stankovich, D. Dikin, R.D. Piner, et al., Carbon **45** (7), 1558 (2007).
7. J. Li, B. Zhang, L. Li, H. Ma, M. Yu, and J. Li, Radiat. Phys. Chem. **94**, 80 (2014).
8. K. S. Novoselov, Science **306** (5), 666 (2004). https://doi.org./10.1126/science.1102896
9. H. Li, Science **342** (6154), 95 (2013).
10. W. Gao, *Graphene Oxide* (Springer-Verlag, 2015). https://doi.org/10.1007/978-3-319-15500-5_3
11. C. Yang, Y. Chen, J. Jiang, and Z. Ao, Solid State Commun. **227**, 23 (2016).
12. S. B. Jo, J. Park, W. H. Lee, K. Cho, and B. H. Hong, Solid State Communications **152** (15), 1350 (2012).
13. C. Dean, A.F. Yung, L. Wang, et al., Solid State Commun. **152**, 1275 (2012).
14. H. Feng, R. Cheng, X. Zhao, X. Duan, and J. Li, Nat. Commun. **4**, 1539 (2013).
15. Y. Caglar, S. Ilican, and M. Caglar, Eur. Phys. J. B **58** (3), 251 (2007).
16. J. Song, X. Wang, and C.-T., J. Nanomater. **2014**, 7 (2014).
17. Y.-K. Kim, H. Jang, and K. Kang, Thin Solid Films **636**, 359 (2017).
18. A. Ulman, Chem. Rev. **96** (4), 1533 (1996).
19. H. R. Thomas, Chem. Mater. **25** (18), 3580 (2013).
20. I. Jung, et al., Nano Lett. **7** (12), 3569 (2007).
21. H. Yang, H. Hu, Y. Wang, and T. Yu, Carbon **52**, 528 (2013).
22. A. Gray, M. Balooch, S. Allegret, S. De Gendt, and W.-E. Wang, J. Appl. Phys. **104** (5), 053109 (2008).

23. I. Jung, Matthias Vaupel, Met'yu Pelto, et al., J. Phys. Chem. C **112** (23), 8499 (2008).
24. Y. Shen P. Zhou, Q.-Q. Sun, et al., Appl. Phys. Lett. **99** (14), 141911 (2011). https://doi.org/10.1063/1.3646908
25. V. Kravets, A.N. Grigorenko, R. Raveendran-Nair, et al., Phys. Rev. B **81** (15), 155413 (2010).
26. K. P. Loh, Q. Bao, G. Eda, and M. Chhowalla, Nat. Chem. **2** (12), 1015 (2010).
27. M. K. Shin, Bommy Lee, Shi Hyeong Kim, et al., Nat. Commun. **3**, 650 (2012).
28. D. C. Marcano D. C., Kosynkin, D. V., Berlin, et al., ACS Nano **4** (8), 4806 (2010).
29. R. Krishna and E. Titus, Appl. Surf. Sci. **424**, 87 (2017).
30. U. Holzwarth and N. J. N. n. Gibson, Nat. Nanotechnol. **6** (9), 534 (2011).
31. P. Paufler, C. S. Barrett, and T. B. Massalski, *Structure of Metals* (Pergamon Press, New York, Toronto, Sydney, Paris Frankfurt/M, 1980).
32. Tabellen und über 1400 Literaturhinweise. Preis US $ 20, Kristall Technik **16** (9), 982 (1981).
33. J. Chen, B. Yao, C. Li, and G. Shi, Carbon **64**, 225 (2013).
34. K. N. Kudin, B. Ozbas, H. C. Schniepp, R. K. Prud'Homme, I. A. Aksay, and R. Car, Nano Lett. **8** (1), 36 (2008).
35. O. Akhavan, E. Ghaderi, E. Hashemi, and R. Rahighi, Ultra-sensitive detection of leukemia by graphene, Nanoscale **6** (24), 14810 (2014).
36. Z. Lin, B. R. Carvalho, Ethan Kahn, et al., Defect engineering of two-dimensional transition metal dichalcogenides, 2D Mater. **3** (2), (2016).
37. S. Ghosh, Ganesan Karuppiah, S.R. Mathews, et al., Appl. Surf. Sci. **349**, 576 (2015).
38. A. J. M. Giesbers, P. C. P. Bouten, J. F. M. Cillessen, Leendert Van der Tempel, et al., Solid State Commun. **229**, 49 (2016).
39. E. El-Menyawy, I. Zedan, and A. Azab, J. Alloys Compd. **695**, 3429 (2017)
40. P. Jalkanen, S. Kulju, K. Arutunov, et al., Thin Solid Films **519** (11), 3835 (2011). Source: arXiv. https://doi.org/10.1016/j.tsf.2011.01.238
41. Y. Shen, Peng Zhou, Q.-Q. Sun, et al., Optical investigation of reduced graphene oxide by spectroscopic ellipsometry and the band-gap tuning, Appl. Phys. Lett. **99** (14), (2011). https://doi.org/10.1063/1.3646908
42. H. Murmann, Z. Phys. **101** (9), 643 (1936).
43. I. Konstantinov, T. Babeva, and S. Kitova, PubMed **37** (19), 4260 (1998). https://doi.org/10.1364/AO.37.004260
44. S. Wemple and M. DiDomenico, Phys. Rev. B **3** (4), 1338 (1971).
45. R. P. Feynman, R. B. Leighton, and M. Sands, *The Feynman Lectures on Physics, V. I: The New Millennium Edition: Mainly Mechanics, Radiation, and Heat* (Basic Books, 2011).
46. M. El-Nahass, M. Ali, and I. Zedan, J. Lumin. **151**, 143 (2014).